Porous Anodic Alumina Template Formation: Deposition Technique Dependence

S. Upreti[1*], K. Mukherjee[1], M. Palit[2], A. Bag[1], S. Mallik[1], S. Chattopadhyay[2, 3], and C. K. Maiti [1]
[1]*VLSI Eng. Lab., Dept. of Electronics and ECE, Indian Institute of Technology, Kharagpur 721302, India*
[2]*Centre for Research in NanoScience & Nanotechnology, University of Calcutta, Kolkata 700098, India*
[3]*Department of Electronic Science, University of Calcutta, Kolkata 700009, India*
[*]E-mail: (s.upreti29@gmail.com)

***Abstract*—Porous anodic alumina (PAA) oxide layers have been deposited on TiN/SiO_2/Si by both the vacuum evaporation (VE) and RF magnetron sputtering (MS) techniques. The deposition technique dependence of the pore size at the surfaces of the anodic aluminum oxide (AAO) membranes has been investigated after two step anodization process. The nanochannel arrays of AAO membranes were characterized with scanning electron microscopy (SEM), atomic force microscopy (AFM) and Fourier transform infrared attenuated total reflectance (FTIR-ATR) analysis. Chemical composition and film structural properties were investigated by x-ray photoelectron spectroscopy (XPS) and high resolution x-ray diffraction (HR-XRD) analyses. It is shown that uniform pore density in AAO templates is obtained using Al films deposited using RF sputtering technique.**

***Index Terms*— AAO, PAA, RF magnetron sputter, Vacuum evaporation.**

I. INTRODUCTION

Nanotechnology has emerged as the future of electronic development with applications drawing from vastly different fields encompassing applied physics and chemistry, electrical, computer science and mechanical engineering, sensor, memory and biological technology [1-3]. Fabrication of nanocomposites is a major challenge that the industry faces today and the development of appropriate and specialized templates is a priority. Surface processing by the formation of thick barrier aluminum oxide has been historically, comprehensively exploited by the industries [4]. Porous anodic alumina (PAA) templates have recently started attracting attention owing to its inexpensive method of fabrication; it facilitates self-organized production without the use of expensive lithographical tools such as e-beam lithography. The PAA has been favored due to its potential application as a scaffold platform in optoelectronic, sensor, magnetic and electronic devices [5-8]. Free standing open pores with high aspect ratio have been profoundly studied for their use as molds to synthesize nanoscale metal, semiconductor and insulator arrays deposited by various methods like chemical bath deposition, atomic layer deposition and electrodeposition [9-14]. CNT, Si and ZnS nanowires have been fabricated [15-17] with remarkable improvement observed in their functionality and properties due to the quantum size effect.

Masuda *et al.* [18] in 1995 reported superior (highly ordered) porous oxide film array using relatively inexpensive two-step potentiostatic method of anodization of Al which yields an ideal honeycomb structure and organized cell arrangement on longer duration of anodization at 40V. These hard templates having homogeneous morphology exhibit parallel pore growth perpendicular to the surface of template.

Self-aligned PAA template formation is a complex electro-chemical process which results in compact honeycomb cell structure with perfectly aligned cylindrical pores having diameters ranging from several hundred down to several tens of nanometers. Density and geometry can be controlled through the anodization parameters such as acid type, concentration, bath temperature, time, current and voltage [4, 19, 20]. The electrolyte pH majorly determines whether the anodized layer will be porous (<5) or barrier type (>7) whereas the acid species determine the size and geometrical arrangement of the ordered nanohole array. The porous membrane formed by anodization at temperatures above 60°C were thin, fragile and non-protective, while anodization at low temperatures typically between 0 to 5°C results in thick, compact and hard oxides [21]. Apart from electrolyte pH, anodization time, voltage and current; the nucleation, growth and size of hemispherical shaped pores are dictated by the effects of random surface defects, such as pits, impurities, scratches and grain boundaries. These are reported to be the preferred sites for the hemispherical depressions and hence influence the PAA architecture during anodization process [22-24]. PAA template is synthesized by maintaining conditions of high voltage and low current with acidic electrolytes used for pore generation majorly being oxalic, phosphoric and sulfuric acid with oxalic acid yielding superior porosity and regularity [25]. Large domains of defect free regions appear though significant defects are found at the boundaries of these domains. Membranes anodized in sulfuric acid have been found to exhibit lower flexibility, hardness and abrasion resistance while anodization in phosphoric acid results in significantly higher cell or pore diameters.

Despite extensive investigation into the formation mechanism of PAA, the exact mechanism of pore formation in AAO is still under contention though the electrolyte's potential to perpetuate a sturdy flow of the Al^{3+} ions into the electrolyte from the metal substrate is considered to be the most decisive factor for the generation of porous oxide. The growth of aluminium oxide at the metal/oxide interface is due to transport of Al^{3+}, OH^- and O^{2-} ions within the alumina film. Loss of Al^{3+} ions is controlled by the dual mechanism of direct discharge due to applied field and the dissolution of the accumulating oxide layer. In the regions with higher current density, under the influence of applied electric field, a larger dissolution rate can exist. It has been reported by Nielsch *et al.* that 10% of porosity is required independent of the anodization conditions to form an ordered porous hexagonal array [26].

V. K. Jain and A. Verma (eds.), *Physics of Semiconductor Devices*, Environmental Science and Engineering,
DOI: 10.1007/978-3-319-03002-9_187,

Self-assembly of the array is driven by the repulsive forces between neighboring pores. Volumetric expansion caused elastic stress controls the expanse of the uniformity and creates the perfect cylindrical and hexagonal arrangement in AAO self-organization process; depending upon the fabrication constrains, pore densities range from 10^8 to 10^{12} pores per cm^2 [27]. The type of Al substrate undergoing anodization is also a dominant factor in regulating the pore or cell arrangement and uniformity. While it has been proved that Al films deposited by vacuum evaporation have a more granular and rough microstructure while magnetron sputtering produces a more homogeneous and microhard surface, the effect of these structural differences on the morphology of the respective anodized films is yet to be established [28].

This paper investigates the subsequent microstructure of both vacuum evaporated (VE) and magnetron sputtered (MS) aluminum thin films used for PAA array formation. Deposition dependence is further investigated under constant electrolytic conditions and anodization duration for profoundly understanding AAO characteristics in terms of its morphology and pore diameters.

II. EXPERIMENTAL DETAILS

This investigation is performed using p-type Si <100> wafer of resistivity of 15-20 Ω-cm, as starting substrate. After standard cleaning (RCA) process, wet thermal oxidation is employed to grow ~ 250-300 nm SiO_2 layer for substrate isolation, maintaining O_2 gas flow at ~10^3 cc/min and temperature about 900°C. TiN layer was deposited through RF magnetron sputtering on the SiO_2/Si structure in Ar ambient for 10 minutes to serve as bottom electrode and strengthen adhesion to Al. The working pressure during deposition was kept at ~1.3 mbar with 100 W RF power, then the formed sample is ready for subsequent Al coating through magnetron sputtering (MS) and vacuum evaporation (VE).

TiN/SiO_2/Si substrate is subjected to RF sputter for Al deposition, keeping power at 100 W and working pressure at ~1.3 mbar in presence of unreactive Ar gas. Aluminium is also deposited on an identical sample through VE; pressure of deposition chamber is kept at ~10^{-6} mbar.

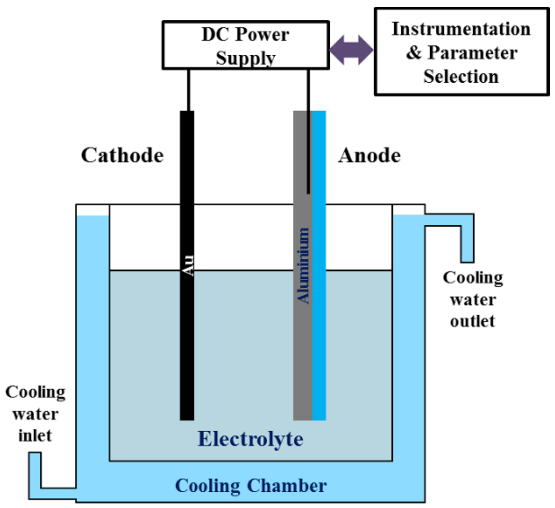

FIG.1. Schematic of the experimental setup used to produce PAA.

Schematic of the experimental setup of anodization used for the fabrication of PAA is shown in Fig. 1. The RF and VE samples are subjected to the first step of anodization in 0.3 M oxalic acid when a 40V dc bias is applied for 30 minutes; then the anodized film is removed using etchant solution consisting of phosphoric acid (wt. 6%) and chromic acid (wt. 2%) at 60°C for 1 min in order to produce hemispherical depressions on the surface and obtain a consistent and uniform nucleation array through self-ordered pore formation. The second anodization step was performed to obtain electrochemically treated samples under similar atmosphere for 2 hours. The anodization process was performed in a chamber maintained at ~5°C, necessary for the fabrication of the porous membrane.

III. RESULTS & DISCUSSIONS

Agilent HP 34401A digital multimeter is used for monitoring current in the electrolysis system. LabVIEW program was used for data acquisition through monitoring the current, voltage and time in the anodization cell. Figure 2 shows different stages through the typical current vs. time (*I-t*) behavior exhibited in the first step of anodization of both the RF and VE samples. Influence of the Al layer deposition method is investigated by *I-t* graph; RF sputtered Al layer on anodization exhibits five different regions while for the VE sample, the plot displays just the first four regions.

In the first stage of anodization of the RF sample; initial conductivity of the sample is high which drastically reduces with time as the initial surface devoid of any oxide layer, forms an even oxide on the entire surface of the substrate within a few minutes or seconds. Increase in anodization current testifies to the initiation of hemispherical depressions by dissolution of the oxide layer at random nucleation sites in second stage, the increase in current and thus decrease in overall resistance occurring as a result of reduction of the oxide layer thickness; this stage lasts for a few minutes. In third stage of the anodization process equilibrium is achieved between dissolution and oxide formation and self-ordered pore formation is exhibited at nucleated sites with pore diameter and cell size getting regulated. With the completion of third stage current starts to reduce gradually and reaches

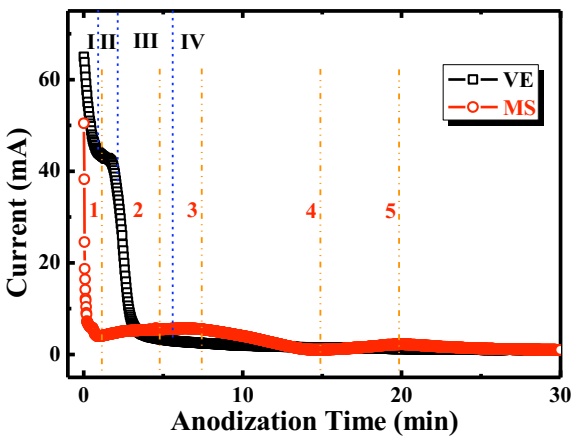

FIG.2. *I-t* curves of first step anodization of AAO/TiN/SiO_2/Si for vacuum evaporated and RF sputtered samples.

close to zero, as the metal/oxide interface reaches the bottom TiN layer. Al present on the substrate is consumed to produce a transparent oxide membrane; fourth stage can extend from several minutes to hours. Due to disruption of the barrier oxide, current increase is established during the fifth stage of anodization. In this step electric field assisted dissolution creates void in the inverted barrier layer at the nucleation sites, most probably due to oxygen bubbles at the PAA/TiN interface [29].

I-t behavior of VE samples demonstrates only the first four stages of anodization. Stage I is the formation stage where anodization at constant voltage results in consistent oxidation of the substrate's surface demonstrated by an acute fall in the value of current. Abrupt increase in current is observed in stage II for a few minutes, surface irregularities and defects primarily determine the intensity of electric field on the oxide layer, resulting in electric field assisted dissolution. Due to larger grain size and rough microstructure of the deposited Al layer, dissolution starts significantly earlier, even before the oxide layer has spread uniformly in contrast with earlier RF sputtered sample. Poor quality of the vacuum evaporated Al sample results in the precocious dissolution, as a result of which, the rise in the current is exhibited. Stage III begins with the completion of the ongoing oxidation process disrupted by the dissolution, within few minutes the equilibrium is achieved in oxidation and dissolution; further anodization causes migration of oxide ions from the pore's tip with high electric field towards the pore wall. PAA templates thus formed are not uniform or ordered. Stage IV comprises the prolonged oxidation to develop self-aligned, regular pore formation, the oxidation reaches completion and current continuously diminishes finally reaching about zero.

The chemical bonding states of PAA membrane was investigated by x-ray photoelectron spectroscopy (XPS) analysis. The XPS measurements were performed under an ultra-high vacuum ($\sim 10^{-10}$ torr) conditions at room temperature using VG Microtech ESCA-2000 XPS system. The data acquisition was done using MgKα (1253.6 eV) excitation source radiation at an angle of 30° between the analyzer axis and the sample normal with a pass energy of 50 eV with an energy resolution of 0.1 eV. In Fig. 3a Al*2p* spectra is displayed with peak corresponding to the Al-O bonding (74.6 eV). O*1s* spectrum is shown in Fig. 3b, it consists of the main peak at 531.3 eV for O*1s* of Al-O bond. Electrochemical formation of Al_2O_3 can deduced from the XPS analysis.

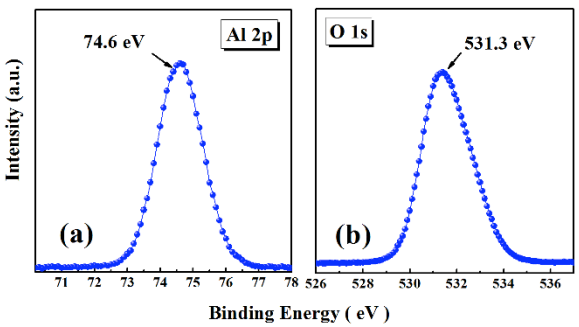

FIG.3. XPS of (a) Al*2p* electrons and (b) O*1s* electrons in the AAO layer.

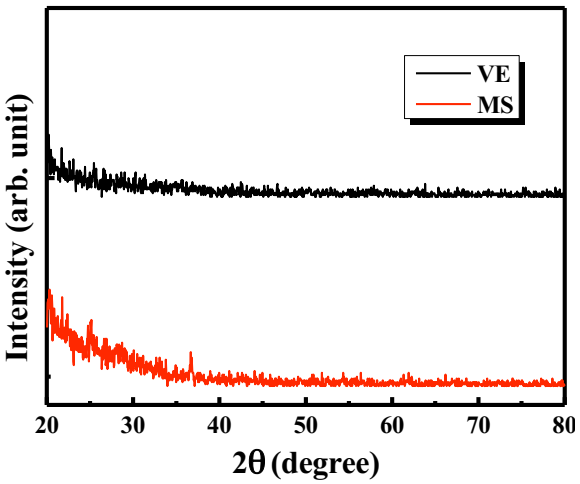

FIG.4 X-ray diffraction pattern of anodized RF sputtered (MS) and vacuum evaporated (VE) aluminum.

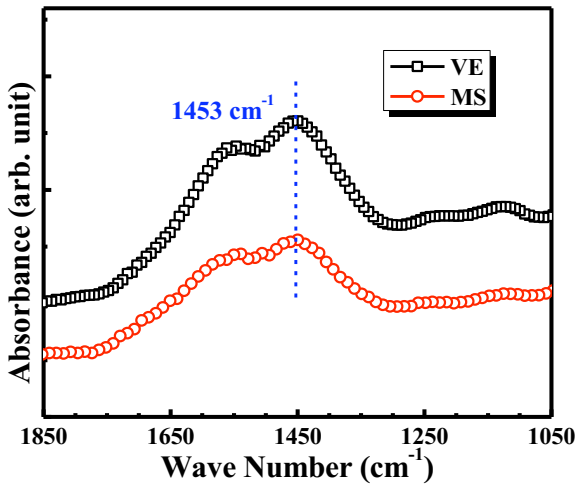

FIG.5 FTIR-ATR spectra of anodized RF sputtered (MS) and vacuum evaporated (VE) aluminum.

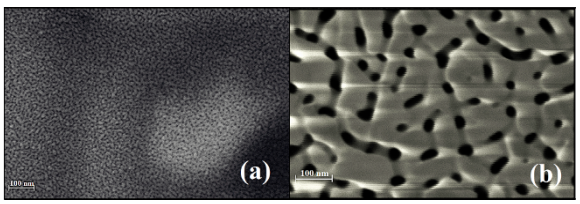

FIG.6. SEM images for (a) MS and (b) VE deposited samples after two step anodization.

In order to examine the crystalline properties of the as grown AAO, HR-XRD analysis was carried out using Panalytical High Resolution XRD, PW 3040/60 with Cu-K_α radiation at 40 kV and 300 mA, and the x-ray incident angle at 2° (Grazing angle). GIXRD data were recorded at 20mA in the 2θ scanning range of 20 to 80° using a constant step width of 0.05°. Figure 4 shows the XRD patterns of as-grown AAO

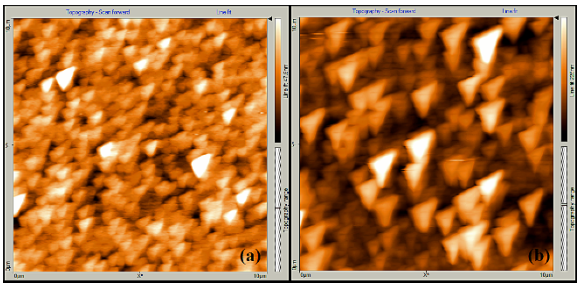

FIG.7. AFM 2D topology of electrochemically treated AAO/TiN on SiO_2/Si films are grown from (a) magnetron sputtering and (b) vacuum evaporation.

films where the lack of any diffraction peak indicates that the AAO film is amorphous in nature.

The structural analysis of the as grown PAA was performed using FTIR-ATR (Agilent Cary 630) for wave numbers ranging from 3200 to 700 cm^{-1}. Figure 5 shows the measured FTIR-ATR spectra of the both MS and VE PAA samples. The spectrum of the measured AAO membrane exhibits a peak at 1453 cm^{-1}, which is close to the reported values [30,31], signifying the formation of Al_2O_3 after the anodization under established electrochemical conditions.

In order to confirm the formation of ultra-small nanopores, we used SEM (Zeiss Auriga FIB-SEM) to characterize the PAA samples. The SEM images of two step anodized MS and VE samples show that the pore proportions are substantially higher in the VE samples as shown in Figs. 6a and 6b, respectively. This may be due to the coarser, non-homogeneous and granular surface coating having pores and cracks, resulting from vacuum evaporation of Al. Because of the substantially larger number of defects or pores in the surface topology of the VE samples, pore nucleation occurs at these defect sites readily and randomly. Inhomogeneous sputtering of TiN cannot be the reason for defects because the MS sample was also prepared in the same way, and no porosity in Al structure was observed. Irregular pore formation is observed in VE sample in comparison with MS samples where even and uniform distribution is observed owing to the periodic and highly ordered fissure array that forms the nucleation sites for the AAO after the first anodization step. This phenomenon is also observed from AFM (NanoSurf EasyScan 2) surface analysis as shown in Figs. 7a and 7b after the second anodization. To understand the surface morphology the AFM study was performed in non-contact mode (Si_3N_4 tip) with a scanning area of 10μm×10μm. Measurement was done at multiple locations for better accuracy. The microstructure of MS sample showed less surface roughness compared to VE sample.

IV. CONCLUSIONS

Growth characteristics of porous anodic alumina fabricated from Al films deposited using magnetron sputtering and thermal evaporation are reported. The formation of PAA membrane on both the samples is verified by SEM and AFM; similar chemical composition is also established by XPS and FTIR-ATR. The results of the investigation reveal that the ultra-fine Al coating with microhardness is produced by RF sputter thus anodized sample exhibits superior and ordered pore arrays. The pore size, uniformity and density distribution is found to be more controllable and favorable in case of the RF sputtered Al films.

V. REFERENCES

[1] S. Ramakrishna, M. Ramalingam, T. S. S. Kumar, and W. O. Soboyejo, *Biomaterials: A Nano Approach*, (CRC Press/Taylor & Francis, FL, USA, 2010).
[2] R. S. Greco, F. B. Prinz, R. L. Smith, *Nanoscale Technology in Biological Systems*, (CRC Press, FL, USA, 2005).
[3] M. G. Lines, *J. Alloys Compd.*, **449**, 242 (2008). [doi:10.1016/j.jallcom.2006.02.082]
[4] G. E. Thompson, *Surface characteristics of aluminium and aluminium alloys*, (TALAT Lecture **5101**, European Al Ass, 2004). [http://core.materials.ac.uk/repository/eaa/talat/5101.pdf]
[5] M. Saito, M. Kirihara, T. Taniguchi, and M. Miyagi, *Appl. Phys. Lett.*, **55**, 607 (1989). [doi:10.1063/1.101572]
[6] F. Favier, E. C. Walter, M. P. Zach, T. Benter, and R. M. Penner, *Science*, **293**, 2227 (2001). [doi: 10.1126/science.1063189]
[7] S. Manalis, K. Babcock, J. Massie, V. Elings, and M. Dugas, *Appl. Phys. Lett.*, **66**, 2585 (1995). [doi:10.1063/1.113509]
[8] D. H. Cobden, *Nature*, **409**, 32 (2001). [doi:10.1038/35051205]
[9] S.-Z. Chu, K. Wada, S. Inoue, S.-I. Todoroki, Y. K. Takahashi, and K. Hono, *Chem. Mater.*, **14**, 4595 (2002). [doi:10.1021/cm020272w]
[10] S. Phok, S. Rajaputra, and V. P. Singh, *Nanotechnol.*, **18**, 475601 (2007). [doi:10.1088/0957-4484/18/47/475601]
[11] L. Velleman, G. Traini, P. J. Evans, A. Atanacio, J. G. Shapter, and D. Losic, in Proc. *SPIE 7267, Smart Materials V*, 72670S (2008). [doi:10.1117/12.810716]
[12] C.-L. Xu, H. Li, G.-Yu Zhao, and H.-L. Li, *Appl. Surf. Sci.*, **253**, 1399, (2006). [doi:10.1016/j.apsusc.2006.02.056]
[13] H. Zhang, X. Ma, J. Xu, J. Niu, J. Sha, and D. Yang, *J. Cryst. Growth*, **246**, 108 (2002). [doi:10.1016/S0022-0248(02)01900-0]
[14] J. Elam, J. A. Libera, P. C. Stair, and M. J. Pellin, *ECS Trans.*, **11**, 177 (2007). [doi:10.1149/1.2779082]
[15] H. Masuda, K. Fukuda, *Science*, **268**, 1466 (1995). [doi:10.1126/science.268.5216.1466]
[16] Y. S. Shin, J. H Yang, C.-Y. Park, M. H. Kwon, J.-B. Yoo, and C. W. Yang, *Jpn. J. Appl. Phys.*, **45**, 1869 (2006). [doi:10.1143/JJAP.45.1869]
[17] L. Mengke, W. Chengwei, L. Hulin, *Chin. Sci. Bull.*, **46**, 1793 (2001). [doi:10.1007/BF02900552]
[18] J. X. Ding, J. A. Zapien, W. W. Chen, Y. Lifshitz, S. T. Lee, and X. M. Meng, *Appl. Phys. Lett.*, **85**, 2361 (2004). [doi:10.1063/1.1791326]
[19] S. Shingubara, *J. Nanopart. Res.*, **5**, 17 (2003). [doi:10.1023/A:1024479827507]
[20] H. Chik, and J. M. Xu, *Mat. Sci. Eng R*, **43**, 103 (2004). [doi:10.1016/j.mser.2003.12.001]
[21] G. E. J. Poinern, N. Ali, and D. Fawcett, *Materials*, **4**, 487 (2011). [doi:10.3390/ma4030487]
[22] G. E. Thompson, Y. Xu, P. Skeldon, K. Shimizu, S. H. Han, and G. C. Wood, *Philos. Mag. B*, **55**, 651 (1987). [doi:10.1080/13642818708218371]
[23] S. J. Garcia-Vergara, L. Iglesias-Rubianes, C. E. Blanco-Pinzon, P. Skeldon, G. E. Thompson, and P. Campestrini, *Proc. R. Soc. A*, **462**, 2345 (2006). [doi:10.1098/rspa.2006.1686]
[24] T. P. Hoar, and J. Yahalom, *J. Electrochem. Soc.*, **110**, 614 (1963). [doi:10.1149/1.2425839]
[25] N.-Q. Zhao, X.-X. Jiang, C.-S. Shi, J.-J. Li, Z.-G. Zhao, and X.-W. Du, *J Mater Sci*, **42**, 3878 (2007). [doi:10.1007/s10853-006-0410-3]
[26] K. Nielsch, J. Choi, K. Schwirn, R. B. Wehrspohn, and U. Gösele, *Nano Lett.*, **2**, 677 (2002). [doi:10.1021/nl025537k]
[27] H.-S. Seo, S.-W. Jee, and J.-H. Lee, *J. Korean Phys. Soc.*, **51**, L1863 (2007). [doi:10.3938/jkps.51.1863]
[28] H. Garbacz, P. Wieciński, B. Adamczyk-Cieślak, J. Mizera, and K.J. Kurzydłowski, *J. Microsc.*, **237**, 475 (2010). [doi:10.1111/j.1365-2818.2009.03297.x]
[29] P. Liu, V. P. Singh, and S. Rajaputra, *Nanotechnology*, **21**, 115303 (2010). [doi:10.1088/0957-4484/21/11/115303]
[30] S. K. Panda, D. Han, H. Yoo, H. Shin, H. Park, and J. Xu, *Electrochem. Solid-State Lett.*, **14**, E21 (2011). [doi:10.1149/1.3569112]
[31] S. D. Ebbesen, B. L. Mojet, and L. Lefferts, Langmuir, **24**, 869 (2008). [doi:10.1021/la7027725]